analytical chemistry

Article

pubs.acs.org/ac

Ion Permeability of the Nuclear Pore Complex and Ion-Induced Macromolecular Permeation as Studied by Scanning Electrochemical and Fluorescence Microscopy

Jiyeon Kim,[†,#] Anahita Izadyar,[§,#] Mei Shen,[¶] Ryoichi Ishimatsu,[‡] and Shigeru Amemiya*

Department of Chemistry, University of Pittsburgh, 219 Parkman Avenue, Pittsburgh, Pennsylvania 15260, United States

ABSTRACT: Efficient delivery of therapeutic macromolecules and nanomaterials into the nucleus is imperative for gene therapy and nanomedicine. Nucleocytoplasmic molecular transport, however, is tightly regulated by the nuclear pore complex (NPC) with the hydrophobic transport barriers based on phenylalanine and glycine repeats. Herein, we apply scanning electrochemical microscopy (SECM) to quantitatively study the permeability of the NPCs to small probe ions with a wide range of hydrophobicity as a measure of their hydrophobic interactions with the transport barriers. Amperometric detection of the redox-inactive probe ions is enabled by using the ion-selective SECM tips based on the micropipet- or nanopipet-supported interfaces between two immiscible electrolyte solutions. The remarkably high ion permeability of the NPCs is successfully measured by SECM and theoretically analyzed. This analysis demonstrates that the ion permeability of the NPCs is determined by the dimensions and density of the nanopores without a significant effect of the transport barriers on the transported ions. Importantly, the weak ion−barrier interactions become significant at sufficiently high concentrations of extremely hydrophobic ions, i.e., tetraphenylarsonium and perfluorobutylsulfonate, to permeabilize the NPCs to naturally impermeable macromolecules. Dependence of ion-induced permeabilization of the NPC on the pathway and mode of macromolecular transport is studied by using fluorescence microscopy to obtain deeper insights into the gating mechanism of the NPC as the basis of a new transport model.

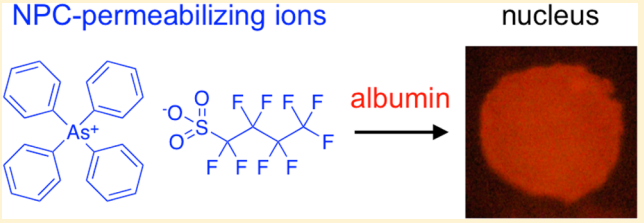

Molecular transport between the nucleus and cytoplasm of a eukaryotic cell is solely controlled by the nuclear pore complex (NPC).[1] The NPC plays imperative roles in gene expression[1,2] and gene delivery[3] to be linked to many human diseases and their therapeutics.[4] Structurally, the NPC is composed of the multiple copies of the distinct 30 proteins called nucleoporins (nups) to form a nanopore with an inner diameter of ∼50 nm along a length of ∼35 nm through the double-membraned nuclear envelope (NE).[5] This large nanopore is highly attractive for gene therapy and nanomedicine, which require the efficient and safe nuclear import of the large conjugates of nucleic acids with polymers,[3] nanoparticles,[6] etc., as vectors. This chemical task, however, is very challenging because the NPC usually mediates the passive transport of only small molecules and proteins with molecular weights of <∼40 kDa.[7] Larger macromolecules are blocked by the hydrophobic transport barriers based on the phenylalanine-glycine (FG) repeats of various nups in the nanopore. Therefore, passively impermeable nuclear proteins must be tagged with nuclear localization signal (NLS) peptides to be chaperoned through the NPC by nuclear transport receptors, i.e., importins. For instance, the NLS of a cargo protein is recognized by importin α (62 kDa), which also binds to importin β (98 kDa) to form a heterodimer with the maximum dimension of 19 nm and a radius of gyration of 5.7 nm.[8] Intriguingly, the even larger importin−cargo complexes can overcome the transport barriers, which has been ascribed to the interactions of importin β with FG repeats.[9,10]

Recent structural[11,12] and transport[13,14] studies of the NPC indicated that the interior of the NPC is concentrically divided into central and peripheral routes by hydrophobic FG-rich nups to spatially regulate molecular transport at the nanometer scale (Figure 1A). For instance, the central zone of the NPC of the *Xenopus laevis* oocyte is occupied by the FG domain that is assembled around Nup98 (Figure 1B) and anchored to cytoplasmic filaments by Nup214.[15] The central domain also includes the helices of the Nup54/Nup62 complex projected from the flexible ring of the Nup54/Nup58 complex.[16] Intrinsically, the FG-based barrier of Nup98 blocks not only passively impermeable macromolecules but also importin−cargo complexes.[17,18] Thus, these complexes are transported through the peripheral route between the central domain and the pore wall.[13,14] In fact, importin-facilitated transport is nearly completely prevented by wheat germ agglutinin (WGA)[19] with a small radius of ∼2.5 nm,[20] which plugs the peripheral zone[21] through binding to the *N*-acetylglucosamine groups of Nup62.[12] This pathway-selective transport, however, is not well understood mechanistically or controllable by an external

Received: November 7, 2013
Accepted: January 25, 2014
Published: January 25, 2014

   dx.doi.org/10.1021/ac403607s | *Anal. Chem.* 2014, 86, 2090−2098

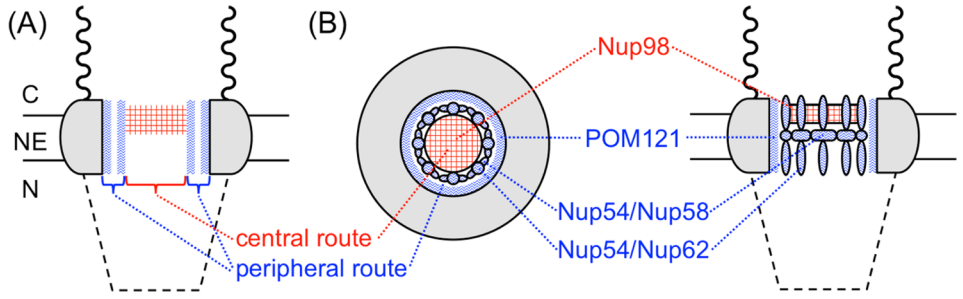

Figure 1. (A) Scheme of the NPC with central (red) and peripheral (blue) barriers. The filaments and basket of the NPC are shown by wavy and dotted lines, respectively. C and N represent cytoplasmic and nucleus sides, respectively. NE is the nuclear envelope. (B) Cytoplasmic top view (left) and side view (right) of the NPC with FG-rich nups forming central (red) and peripheral (blue) barriers.

factor despite its importance for rational design of nuclear gene delivery for therapeutics and other applications.

In this work, we apply scanning electrochemical microscopy[22,23] (SECM) to determine the permeability of the NPCs to small probe ions with a wide range of hydrophobicity as a measure of their interactions with the hydrophobic transport barriers. In contrast to our previous SECM studies of the NPC,[14,24] its permeability to redox-inactive probe ions is measured in this study by using the SECM tips based on the interface between two immiscible electrolyte solutions (ITIES).[25] In comparison to metal SECM tips, the ITIES-based tips have such advantages as diverse ion selectivity,[26,27] robustness,[28] and extremely small size[29] to serve as a powerful tool for biological studies.[30] Specifically, a micro-ITIES is formed at the ~1 μm-diameter tip of the glass pipet filled with a water-immiscible 1,2-dichloroethane (DCE) solution to amperometrically detect an aqueous target ion at nanometer distances from the NE (Figure 2A). The tip−NE nanogaps are

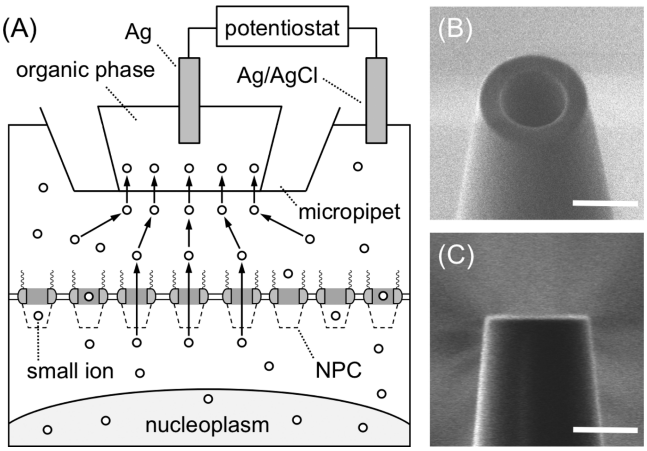

Figure 2. (A) Measurement illustration of the ion permeability of the NE using a micropipet-supported ITIES tip. The nucleus was swollen to detach the NE from the nucleoplasm for smoothening. (B) SEM and (C) FIB images of a milled micropipet. Scale bars, 1 μm.

required for precise SECM measurement of high membrane permeability[27] and are formed by smoothening the rough orifice of a heat-pulled pipet using focused ion-beam (FIB) milling[27,31] (Figure 2B,C). In addition, we apply nanopipet-supported ITIES tips[32,33] to attempt the study of single NPC permeability.

Importantly, this study leads to the novel finding that the NPC is permeabilized with pathway selectivity to naturally impermeable macromolecules in the presence of high concentrations of extremely hydrophobic ions, i.e., tetraphenylarsonium ($TPhAs^+$) and perfluorobutylsulfonate ($PFBS^-$) although their interactions with transport barriers are too weak to be detected by SECM (see Results and Discussion). We employ fluorescence microscopy to demonstrate that the ion-induced nuclear import of bovine serum albumin (BSA; ~67 kDa) is mediated through the peripheral route and is blocked by WGA. In addition, the central route is permeabilized to the importin complex of NLS-tagged BSA, which is no longer blocked by WGA. To explain this pathway- and mode-dependent permeabilization, we propose the new transport model based on distinct structures of central and peripheral transport barriers (Figure 1). Significantly, our model implies that the peripheral route is blocked by more flexible transport barriers to be more readily permeabilized for the efficient nuclear import of therapeutic macromolecules and nanomaterials. We argue that the peripheral route has been explored for gene therapy and nanomedicine although the use of the peripheral pathway has been unnoticed.

EXPERIMENTAL SECTION

Chemicals. Poly(vinyl pyrrolidone) (PVP; average molecular weight, 40 kDa), nonafluorobutanesulfonic acid, $LiPF_6$, tetraphenylarsonium chloride (TPhAsCl), $LiClO_4$, tetrabutylammonium (TBA^+) chloride, 1,2-dichloroethane (DCE), and chlorotrimethylsilane (≥99%) were purchased from Aldrich (Milwaukee, WI). The PF_6 salt of (ferrocenylmethyl)trimethyl ammonium ($FcTMA^+$) was prepared by metathesis of its iodide salt (Strem Chemicals, Newburyport, MA) and NH_4PF_6 (Strem Chemicals). The tetrakis(pentafluorophenyl)borate salt of tetradodecylammonium was obtained by metathesis and used as organic supporting electrolytes. Deionized water (18.2 MΩ·cm; Nanopure, Barnstead, Dubuque, IA) was used to prepare the mock intracellular buffer solution at pH 7.4 containing 90 mM KCl, 10 mM NaCl, 2 mM $MgCl_2$, 1.1 mM EGTA, 0.15 mM $CaCl_2$, and 10 mM HEPES. Furthermore, 15 or 5.5 g/L PVP was added to the buffer solution to prepare an isotonic or a hypotonic solution, respectively.

Nucleus Isolation. The nucleus was isolated from the stage VI oocyte of a female *Xenopus laevis* frog (NASCO, Fort Atkinson, WI).[34] Nucleus isolation was carried out in the isotonic buffer solution using sharp tweezers under a stereomicroscope.[34] Stage VI oocytes were extracted from female *Xenopus* frogs and stored at 18 °C in the modified Barth's solution at pH 7.4 containing 88 mM NaCl, 1.0 mM KCl, 2.4 mM $NaHCO_3$, 0.82 mM $MgSO_4$, 0.33 mM $Ca(NO_3)_2$, 0.41 mM $CaCl_2$, 10 mM HEPES, and 1% penicillin−

dx.doi.org/10.1021/ac403607s | Anal. Chem. 2014, 86, 2090−2098

streptomycin. Fresh oocytes were used for SECM and fluorescence experiments within 3 days of extraction.

Preparation of Pipet-Supported ITIES Tips. Tapered micropipets with an inner tip diameter of 0.6 ± 0.2 μm were obtained by heat-pulling borosilicate glass capillaries (o.d./i.d. = 1.0 mm/0.58 mm, 10 cm in length, Sutter Instrument, Novato, CA) using a CO_2-laser capillary puller (model P-2000, Sutter Instrument). The rough tip end of the pulled micropipets was milled and smoothened by the focused beam of high-energetic gallium ions (100 pA at 30 keV) using a dual beam instrument (SMI3050SE FIB-SEM, Seiko Instruments, Chiba, Japan).[27,31] The outer and inner radii of the milled tips were ∼0.85 and ∼0.5 μm, respectively. The milled micropipets were dried for 2 h under vacuum (∼0.1 Torr) in a desiccator (Mini-Vacuum Desiccator, Bel-Art Products, Pequannock, NJ) and then silanized by introducing 0.5 mL of chlorotrimethylsilane into the desiccator.[32,35] Silanization was performed in the sealed desiccator for 40 ± 10 min depending on the temperature and humidity of the atmosphere. After silanization, the desiccator was purged with N_2 for ∼1 min to remove extra silanization reagent. Similarly, nanopipets were pulled from quartz capillaries (o.d./i.d. = 1.0 mm/0.70 mm, 10 cm in length, Sutter Instrument) and silanized in the vacuum desiccator as reported elsewhere.[32] The silanized pipets with micrometer or nanometer size were filled with 10 μL of a 1,2-DCE solution containing 0.1 M of the organic supporting electrolytes immediately before SECM experiments.

Measurement and Analysis of SECM Approach Curve. SECM approach curves were measured at the NE that was smoothened and stabilized in the recently developed microchamber.[14] The chamber was filled with the mock intracellular buffer solution of a target ion containing 5.5 g/L PVP. The nucleus was swollen in the hypotonic solution to detach the expanding NE from the nucleoplasm. An SECM instrument with closed-loop piezoelectric positioners (CHI 910B, CH Instruments, Austin, TX) was placed on a vibration isolation platform (model 63-533, TMC, Peabody, MA). A two-electrode setup was employed with a 1 mm-diameter Ag wire in a micropipet and a 1 mm-diameter AgCl-coated Ag wire in the buffer solution. An electrochemically etched Pt wire was used as an electrode in the nanopipet.[32,33] The voltammogram of a target ion was obtained by positioning the tip in the bulk solution prior to an approach curve measurement. All electrochemical measurements were taken at room temperature.

An approach curve at either the NE or the Si wafer was analyzed by employing the finite element method to determine NE permeability to a target ion or its diffusion coefficient, respectively.[14] The inner and outer tip radii employed in the finite element analysis were consistent with those determined from the SEM and FIB images of the tip (e.g., Figure 2B and C, respectively).

Fluorescence Transport Assay. General procedures for fluorescence transport assays were reported elsewhere.[14,24] The nucleus was incubated in the isotonic buffer solution of the NPC-permeabilizing ions for 20 min and then in the following transport media for 10 min. The nucleus was rinsed with a small volume of the isotonic solution and transferred to the microchamber filled with the isotonic solution for fluorescence imaging using the inverted microscope equipped with a 4× objective lens (IX-71, Olympus America Inc., Melville, NY). BSA was labeled with trimethylrhodamine isocyanate (Aldrich) and added to the isotonic solution for passive transport assays. The transport medium for facilitated transport contained 0.5 μM sulforhodamine-labeled and NLS-tagged BSA (Aldrich), 0.5 μM importin α_2 (Novus Biological, Littleton, CO), 0.5 μM importin β_1 (Aldrich), and energy mix (2 mM ATP, 25 mM phosphocreatine, 30 units/mL creatine phosphokinase, 200 μM GTP). The permeabilized nucleus was also incubated in the isotonic solution containing 1.0 g/L WGA (Aldrich) for 25 min prior to the transport assays. In addition, impermeability to BSA was recovered by incubating the permeabilized nucleus in the isotonic solution without the permeabilizing ions for 1−2 h.

RESULTS AND DISCUSSION

Hydrophobicity of NPC-Permeabilizing Ions. $PFBS^-$ and $TPhAs^+$ are extremely hydrophobic as confirmed by cyclic voltammetry of their transfer at the micropipet-supported interface between 1,2-DCE and water. The hydrophobicity of $PFBS^-$ is high due to the strong electron-withdrawing effect of fluorine atoms on the sulfonate group, which is weakly hydrated.[36] In addition, $TPhAs^+$ is more hydrophobic than $PFBS^-$, when their hydrophobicity is compared using the $TPhAs^+$−tetraphenylborate assumption.[36] Specifically, both $PFBS^-$ and $TPhAs^+$ give well-defined voltammograms at potentials far from less hydrophobic anions (ClO_4^- and PF_6^-) and cations ($FcTMA^+$ and TBA^+), respectively (Figure 3). For a comparison among the different ions, the current

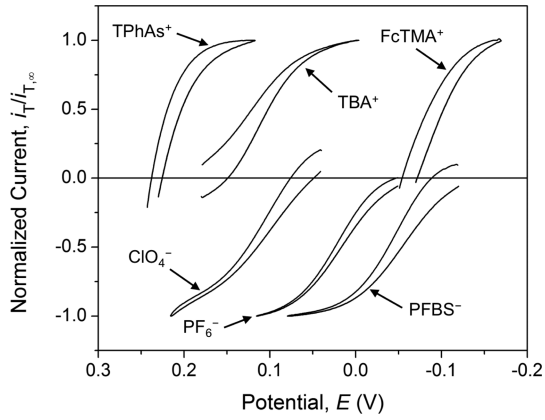

Figure 3. Cyclic voltammograms of various ions at the 1,2-DCE/water interfaces supported at ∼1 μm diameter pipets. Reference electrode, Ag/AgCl. Potential sweep rate, 10 mV/s.

response was normalized against the corresponding limiting current, $i_{T,\infty}$, and plotted against the potential of the organic phase with respect to the aqueous phase, E. The voltammogram of a more hydrophobic cation is seen at the more positive potentials, thereby yielding the order $TPhAs^+$ > TBA^+ > $FcTMA^+$. Inversely, the transfer of a more hydrophobic anion is driven at more negative potentials, which corresponds to the order $PFBS^-$ > PF_6^- > ClO_4^-.

The extreme hydrophobicity of $TPhAs^+$ and $PFBS^-$ was quantitatively assessed from the half-wave potentials of the voltammograms by using[36]

$$\frac{P_i}{P_j} = \exp\left[-\frac{zF(E_{i,1/2} - E_{j,1/2})}{RT}\right] \quad (1)$$

where P_i and P_j are the partition coefficients of ions, i and j, with the same charge, z (= +1 or −1), respectively, between the 1,2-DCE phase and the hypotonic buffer solution, and $E_{i,1/2}$

dx.doi.org/10.1021/ac403607s | Anal. Chem. 2014, 86, 2090−2098

and $E_{y1/2}$ are the half-wave potentials of the respective ions as determined from the cyclic voltammograms in Figure 3. $TPhAs^+$ is approximately 10^5 times more hydrophobic than $FcTMA^+$ with a difference of ~300 mV between their half-wave potentials. $PFBS^-$ is approximately 10^3 times more hydrophobic than ClO_4^- with an ~180 mV difference of half-wave potentials. Noticeably, physiological ions in the aqueous buffer solution, i.e., Na^+, K^+, Mg^{2+}, Ca^{2+}, and Cl^- (see Experimental Section), are too hydrophilic to be transferred into the organic phase within the background potential range.

Ion Permeability of the NE. The permeability of the NE to $TPhAs^+$ and $PFBS^-$, as well as to the less hydrophobic ions, was measured by SECM using micropipet-supported ITIES tips. The SECM measurement was carried out as reported elsewhere for Pt tips.[14] The large nucleus (~380 μm in diameter) was isolated from a *Xenopus laevis* oocyte. NE permeability, k_{NE}, was determined from an SECM approach curve to the NE, i.e., a plot of tip current, i_T, versus tip−NE distance, d. To facilitate the close tip approach, the rough and wrinkled NE was expanded, detached from the nucleoplasm, and smoothened (Figure 2A) by swelling the nucleus in a hypotonic buffer solution containing 5.5 g/L PVP. The swelling of the nucleus confirms that the NPC maintained physiological macromolecular impermeability when low concentrations of $TPhAs^+$ and $PFBS^-$ (0.15 and 0.20 mM, respectively) were employed in the SECM study. Additionally, we measured approach curves at the Si wafer to determine the diffusion coefficients of the target ions in the hypotonic buffer solution.

Figure 4A shows SECM approach curves for $TPhAs^+$ at the NE and the Si wafer, as obtained using ~0.9 μm-diameter tips. As the tip approached perpendicularly to the substrates, the tip current decreased from the diffusion-limited current in the bulk solution, $i_{T,\infty}$. The approach curve at the NE, however, was more positive than the purely negative approach curve at the inert Si wafer (solid and dashed lines, respectively). The higher tip current at the NE is due to $TPhAs^+$ transport through the NPCs from the nucleus to the tip as induced by amperometric depletion of $TPhAs^+$ at the tip,[14,24] i.e., SECM-induced transfer[37] (Figure 2A). The experimental approach curve was fitted with a theoretical curve as obtained by employing the finite element method with NE permeability, tip inner and outer radii, and tip position at the zero tip−NE distance as fitting parameters.[14] A good fit was obtained by using a high k_{NE} value of 0.058 cm/s and tip inner and outer radii of 0.45 and 0.77 μm, respectively. In contrast, the experimental approach curve at the Si wafer was fitted with a theoretical negative approach curve, i.e., k_{NE} = 0 cm/s, with tip inner and outer radii of 0.47 and 0.80 μm. The tip radii employed for the theoretical curves were confirmed by SEM and FIB imaging. Remarkably, this analysis also shows that the smooth ~0.9 μm-diameter tips can approach as close as 22 nm from the NE and even closer to the Si wafer, down to a separation of 9 nm. The short distance at the tip−NE contact indicates that the self-standing NE is flat and stable. The nonzero contact distance is likely due to the slight tilt of the tip with respect to the NE. Noticeably, the small contact distance gives a minimal systematic error of ~20% in the permeability value.[14] Specifically, an offset distance of 22 nm at the tip−NE contact can be increased (or decreased) by ~20% to fit the experimental curve with theoretical curves with <20% lower (or higher) permeability values, thereby yielding k_{NE} = 0.058 ± 0.012 cm/s. This precise measurement of NE permeability was also carried out for PF_6^-, ClO_4^-, TBA^+, and $FcTMA^+$. Both

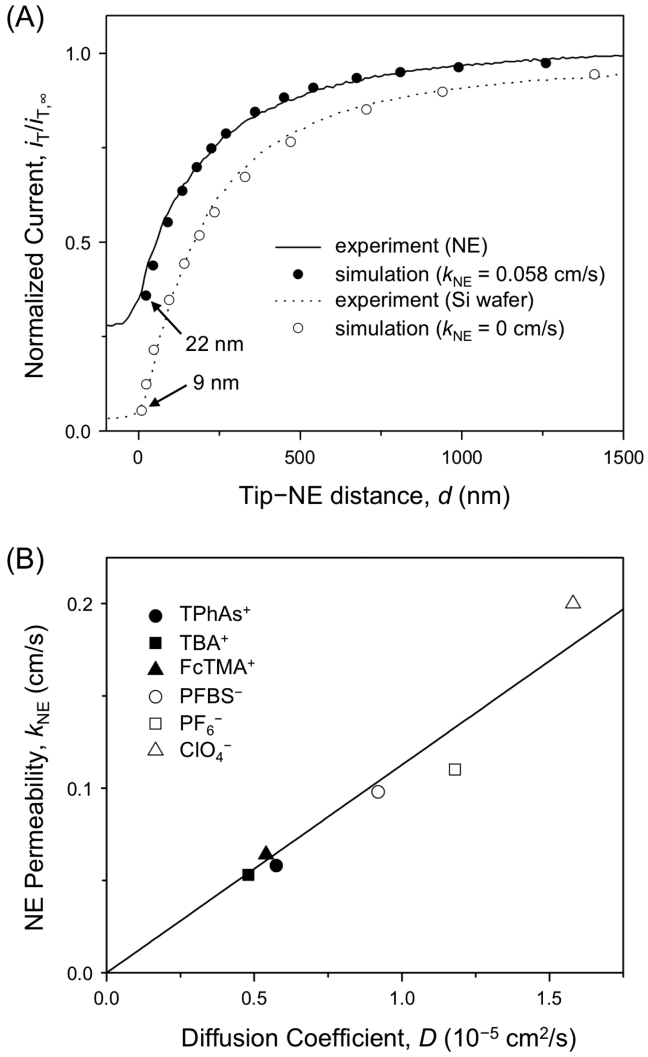

Figure 4. (A) Experimental approach curves for $TPhAs^+$ at the NE and the Si wafer as obtained with micropipet-supported ITIES tips. Tip approach rate, 0.30 μm/s. (B) Plot of the ion permeability of the NE against ion diffusion coefficient. The solid line is the best fit of eq 2 with the experimental plot.

ITIES and Pt[14] tips can detect $FcTMA^+$ to obtain very similar k_{NE} values of 0.064 and 0.059 cm/s, respectively. This result indicates that the tips do not significantly affect NPC permeability.

The permeability data demonstrate that all examined ions freely diffuse through the NPC independently of ion hydrophobicity and ionic charge (Figure 4B). This result indicates that ion−barrier interactions are too weak to be detected by SECM. Nearly identical k_{NE} values were obtained for $TPhAs^+$ and $FcTMA^+$, although their hydrophobicity differs by 5 orders of magnitude. Moreover, NE permeability to all examined cations and anions is controlled by their diffusivity and is proportional to their diffusion coefficients in the hypotonic solution, D. Such a linear relationship is expected when the transported ions freely diffuse through the nanopore without significant interactions with any component in the pore including transport barriers.[14,27] We used effective medium theories to obtain the permeability of a nanoporous membrane to freely diffusing molecules as[14]

dx.doi.org/10.1021/ac403607s | *Anal. Chem.* 2014, 86, 2090−2098

$$k_{NE} = \frac{2Nr}{2l/\pi r + 1/f(\sigma)}D \quad (2)$$

with

$$f(\sigma) = \frac{1 + 3.8\sigma^{5/4}}{1 - \sigma} \quad (3)$$

where N is pore density, r and l are the radius and length of a cylindrical nanopore, respectively, and σ (= πNr^2) is the porosity of the membrane. The best fit of eq 2 with the plot in Figure 4B gives the slope that is consistent with N = 40 NPCs/μm^2, r = 24 nm, and l = 35 nm. These values are typical for the NPC of the *Xenopus* oocyte nucleus as reported in the literature.[5,38] This nanopore density corresponds to ~25 NPCs under a ~0.9 μm-diameter ITIES tip.

Attempts at Single NPC Study by Nanopipet Tips. We attempted the preliminary study of single NPC permeability using ~30 nm-diameter ITIES tips. Recently, we employed nanopipet-supported ITIES tips for SECM imaging to quantitatively resolve ion transport through the single nanopores of a silicon membrane[33] as the geometrical model of the NPC.[39] In such SECM measurement, a nanopipet tip must be positioned within a few nanometers from a single nanopore. The resultant higher mass-transport condition across the shorter nanotip−NPC gap should enhance the kinetic effect of transport barriers on the measured permeability of the single NPC in comparison to that of the NE at ~20 nm distances from a submicrometer-size tip.

Our preliminary attempts at single NPC study were limited by two rather interesting observations. First, we found that the nucleus did not swell when ≥10 mM TPhAs$^+$ was added to the extranuclear transport media. The high ion concentration was employed to obtain an easily detectable current response at ~30 nm-diameter nanopipet tips. No swelling of the nucleus is due to permeabilization of the NPC to naturally impermeable macromolecules, e.g., PVP and large nuclear proteins (see the next section for experimental confirmation), which results in an isotonic condition across the NE. Second, ITIES-based nanotips were fouled near the nucleus to yield much lower current responses. It, however, is interesting that the current at the fouling tip decreased stepwise. Figure 5 shows the example of a current response to TBA$^+$ at the tip that was most severely fouled near the nucleus. The number of steps varied with tips.

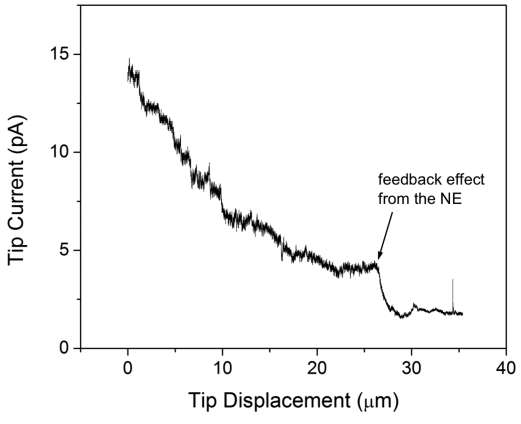

Figure 5. Approach curve at the NE as obtained using the ~30 nm-diameter pipet filled with the 1,2-DCE solution of the organic supporting electrolytes. The external solution was the hypotonic buffer solution of 10 mM TBACl. Tip approach rate, 60 nm/s.

In contrast, tip current was very stable when the tip was positioned in the bulk solution. Considering the small size of the pipet tip (~30 nm diameter), we speculate that each step may correspond to adsorption of one or a few protein molecules at the nanoscale ITIES. Adsorbed protein molecules can partially block the access of TBA$^+$ to the interface to decrease the tip current. In fact, even relatively small proteins with a molecular weight of less than the passive transport limit of the NPC (<40 kDa) are typically adsorbed at the ITIES and rarely extracted into the DCE phase.[40] Moreover, it has been reported that adsorption of single inert nanoparticles on the micrometer-sized electrode shows such a stepwise decrease of a current response.[41,42] Nevertheless, more work is needed to verify the mechanism of nanopipet fouling near the nucleus.

Ion-Induced Macromolecular Transport. We carried out fluorescence transport assays to demonstrate that TPhAs$^+$ and PFBS$^-$ permeabilize the peripheral and central routes of the NPC to naturally impermeable macromolecules. In these assays, rhodamine-labeled BSA (~67 kDa) was used for passive transport and was also tagged with NLS peptides for facilitated transport in the presence of importin α_2 (62 kDa) and importin β_1 (98 kDa). Importin α_2 served as the adaptor that binds to both importin β_1 and the NLS peptide.[43] WGA was used to block the peripheral route,[21] thereby enabling us to identify the permeabilized route.

The hydrophobic ions permeabilize the peripheral route of the NPC to naturally impermeable BSA.[14,24] Significant fluorescence was seen from the nucleus incubated with rhodamine-labeled BSA and 40 mM TPhAs$^+$ or 80 mM PFBS$^-$ (left images in Figure 6A). Anomalous BSA transport was mediated through the peripheral route and was nearly completely blocked by WGA (middle images). This result also demonstrates that the central route was not permeabilized to BSA by TPhAs$^+$ or PFBS$^-$. Noticeably, weak fluorescence was

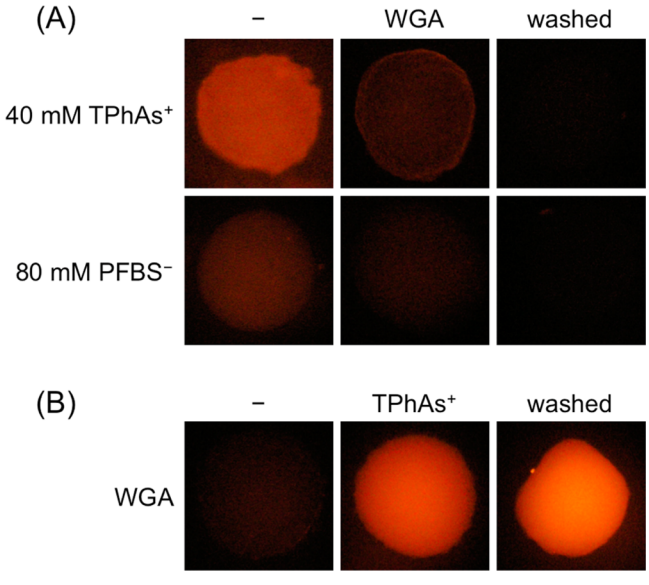

Figure 6. Fluorescence microscopic images of the whole nuclei in the isotonic solution after incubation with (A) rhodamine-labeled BSA and (B) rhodamine-labeled and NLS-tagged BSA and importins. In part (A), the nuclei were preincubated with either TPhAs$^+$ or PFBS$^-$ (left) and, then, with the isotonic solution with (middle) or without (right) WGA. In part (B), the nuclei were preincubated only with WGA (left) or permeabilized by TPhAs$^+$ (middle) and then washed in the isotonic solution (right) before incubation with WGA.

dx.doi.org/10.1021/ac403607s | *Anal. Chem.* 2014, 86, 2090−2098

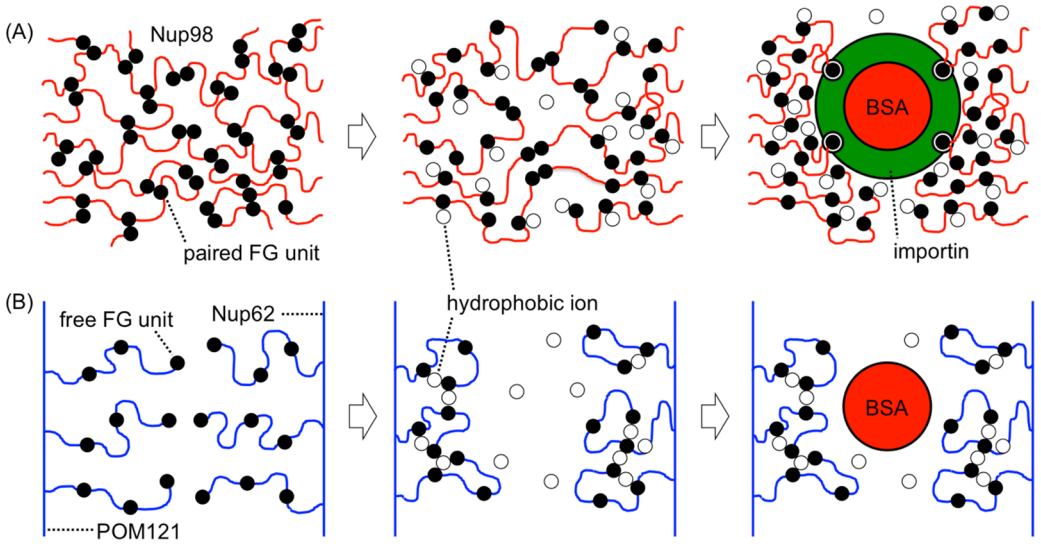

Figure 7. Mechanism of ion-induced permeabilization of (A) central mesh barriers and (B) peripheral polymer-brush barriers to the importin-facilitated transport of NLS-tagged BSA and the passive transport of BSA, respectively.

seen from the surface of the nucleus incubated with WGA and $TPhAs^+$. This weak fluorescence is due to adsorption of rhodamine-labeled BSA at the NPC or the double membrane of the NE, which confirms no nuclear import of BSA.

Permeabilization of the NPC to BSA is ascribed to the cooperative hydrophobic interactions of $TPhAs^+$ and $PFBS^-$ with FG-based barriers through the peripheral route. The interactions are hydrophobic because less hydrophobic cations ($FcTMA^+$ and TBA^+) and anions (ClO_4^- and PF_6^-) did not permeabilize the NPC to BSA. Furthermore, the NPC was impermeable to BSA when the K^+ concentration in the extranuclear buffer solution was increased by 80 mM. This result excludes the possibility that permeabilization of the NPC by the hydrophobic ions is simply due to a change in ionic strength or due to their electrostatic interactions with the charged regions of FG-rich nups.[18] Electrostatic effects are not crucial to permeabilization of the NPC to BSA, which is caused by both anion ($PFBS^-$) and cation ($TPhAs^+$). Moreover, the hydrophobic ion−barrier interactions are cooperative because permeabilization of the NPC to BSA requires the threshold concentrations of the hydrophobic ions as predicted by a recent theory (see below). The threshold concentrations are dependent on ion hydrophobicity and are lower for more hydrophobic $TPhAs^+$ (10 mM) than for $PFBS^-$ (80 mM).

Importantly, the permeabilization of the peripheral route to BSA is reversible and is not due to the substantial loss of transport barriers from the NPC. The permeabilized NPC became impermeable to BSA after the nucleus was washed in the solution free of the hydrophobic ions for 1−2 h, thereby showing no fluorescence (right images in Figure 6A). This slow recovery is due to accumulation of the permeabilizing ions in the nucleoplasm. Complete recovery of impermeability to BSA contrasts to the case of NPC permeabilization by hydrophobic alcohols,[44] which remove Nup98 from the NPC.[12] In addition, such detergents as CHAPS[45] and Triton X[46] dissolve lipids from the double membrane to irreversibly permeabilize the NE.

We further investigated permeabilization of the NPC by $TPhAs^+$ to find that this extremely hydrophobic ion can permeabilize the central route of the NPC to the importin complex of NLS-tagged BSA (Figure 6B). Importin-facilitated transport is naturally mediated through the peripheral route of the NPC and is nearly completely blocked by WGA without $TPhAs^+$ (left image). In contrast, WGA did not prevent the importin-facilitated transport of NLS-tagged BSA in the presence of 40 mM $TPhAs^+$ (middle image), which indicates permeabilization of the central route. Moreover, WGA did not block the importin complex of NLS-tagged BSA after the permeabilized nucleus was incubated in the solution containing no $TPhAs^+$ for 4 h (right image). No recovery of the impermeability of the central route to the importin−BSA complex is not due to the substantial loss of central barriers. The central route of the NPC treated with $TPhAs^+$ is still impermeable to passive BSA transport (middle images in Figure 6A).

Noticeably, ion-induced macromolecule transport is unlikely to be mediated through the double-membraned region of the NE surrounding the NPCs. In fact, the anomalous import of BSA (~67 kDa) into the ion-treated nucleus was blocked by WGA (middle images in Figure 6A), which binds to the periphery of the NPC. The much larger complex of NLS-tagged BSA with importin α and importin β (~230 kDa) is even more unlikely to permeate through the hydrophobic region of the NE. On the other hand, one may argue that a protein molecule may cross the hydrophobic region by forming an electrically neutral and hydrophobic complex with NPC-permeabilizing ions. This transport mechanism is analogous to the response mechanism of a potentiometric protamine sensor based on the extraction of the small protein (4.5 kDa) from an aqueous solution to a hydrophobic polymer membrane.[47] Recent voltammetric/amperometric studies, however, showed that larger proteins including albumin are rarely extracted into the hydrophobic organic media.[40]

Molecular Mechanisms for NPC Permeabilization. The pathway- and mode-dependent permeabilization of the NPC by the hydrophobic ions indicates that the central and peripheral barriers of the NPC must be structurally different. Here, we propose the new model based on two distinct transport barriers, i.e., polymer-brush[9] and mesh[10] barriers for peripheral and central routes, respectively. Uniquely, our synergetic model hypothesizes that polymer-brush and mesh barriers coexist in the single NPC. In fact, it was predicted theoretically that polymer-brush and mesh structures are not mutually exclusive

dx.doi.org/10.1021/ac403607s | Anal. Chem. 2014, 86, 2090−2098

and represent two stable morphologies of the ensemble of FG repeats with different cohesiveness and density.[48] Each barrier structure, however, has been exclusively employed in various transport models, which hypothesize only one pathway for macromolecular transport through the NPC. For instance, it was hypothesized that polymer-brush barriers were formed by the FG nups tethered to the pore wall to entropically control the macromolecular permeability of the central zone of the NPC as the sole pathway.[49] Moreover, the selective phase/hydrogel model hypothesizes that mesh barriers homogeneously distribute in the entire nanopore as the transport pathway.[18]

Coexistence of mesh and polymer-brush barriers through central and peripheral routes, respectively, in our synergetic model is supported by the structural studies of FG-nups. A mesh barrier is formed through the central route by multivalent hydrophobic interactions among the FG repeats of Nup98 (Figure 7A). Tight meshes are formed by Nup98 because cohesion among FG repeats is facilitated in such a crowding zone[50] as the pore center and also because more cohesive GLFG (L, leucine) repeats[11] are incorporated only in Nup98 among the nups of the *Xenopus* oocyte NPC. In contrast, the aqueous peripheral route is covered by FG repeats extending from the periphery of the central FG domain, i.e., the periphery of Nup62, Nup58, and Nup54, and also from the surface of the pore wall, e.g., POM121[7] (Figure 7B). These peripheral FG peptides are less crowding and less interactive to each other, thereby maintaining their intrinsically disordered structure to serve as flexible polymer brushes.

We hypothesize that the NPC-permeabilizing ions weaken the mesh of central barriers (Figure 7A) to mediate importin-facilitated transport. Görlich et al.[51] extensively studied the hydrogels formed by FG nups to propose that the tightest mesh is formed when all cohesive FG units can find sufficiently close binding partners. Thus, the saturated mesh with the minimum size is formed when the concentration of cohesive FG repeats exceeds a critical concentration. Below this concentration, the mesh is undersaturated and contains a significant fraction of unpaired cohesive units, thereby yielding a larger and weaker mesh in comparison to the saturated mesh. We speculate that the NPC-permeabilizing ions interact with the cohesive hydrophobic units of Nup98 to cause the transition of the saturated mesh to an unsaturated state. The resultant larger mesh is still tight and small enough to block BSA. The weakened mesh, however, is further enlarged through interactions with importins to transport their complexes with NLS-tagged BSA.

Anomalous BSA transport through the peripheral route is ascribed to ion-induced compression of peripheral polymer-brush barriers to a lower height state (Figure 7B) as supported by recent theoretical studies.[52,53] Theoretically, such a morphological and height change of a polymer brush can be driven by its weak attractive interactions with multiple nanoparticles. It was predicted that the number of the nanoparticles adsorbed to a plane-grafted polymer-brush layer sharply increases when the nanoparticles in the bulk exceed a certain concentration. This cooperative binding of multiple nanoparticles collapses the polymer layer. Analogously, we speculate that the NPC-permeabilizing ions cooperatively interact with the unpaired cohesive FG units of polymer brushes to compress these barriers. In fact, the resultant permeabilization of the peripheral route to BSA requires threshold ion concentrations as expected theoretically.

Peripheral Route for Efficient Nuclear Import. Our new synergetic model implies that the less tightened peripheral route should be targeted for the efficient nuclear import of macromolecules and nanomaterials for therapeutic and other applications. Flexible polymer-brush barriers through the peripheral route are more readily permeabilized as shown by using the extremely hydrophobic ions. Direct addition of the hydrophobic ions to the cellular media, however, is not optimal for safe nuclear import especially because of their irreversible effect on central barriers, which are crucial to RNA export.[54,55] Covalent modification of a large substance with these NPC-permeabilizing ions is more practical and suitable for safer nuclear import.[56]

Interestingly, the implication of our model is supported by the NLS-independent nuclear import of glycosylated substances as explored for gene therapy and nanomedicine. Remarkably, BSA,[57] plasmid DNA,[58,59] and CdTe/ZnS quantum dots with Stokes radii of up to 6.1 nm[60] were glycosylated to be imported efficiently into the nuclei of living cells. We argue that the nuclear import of glycosylated substances is somehow mediated through the peripheral route because it is prevented by WGA.[57]

■ CONCLUSIONS

This work exemplifies the power of ITIES-based SECM as a quantitative chemical tool for the in situ and real-time study of biological systems.[30] The ion-selective micropipet tips enabled us to quantitatively monitor the redox-inactive probe ions in the presence of physiological ions and leaching nuclear proteins. The use of the nonphysiological probe ions eventually led to biologically and therapeutically significant discovery of the NPC-permeabilizing ions and also to experimental observation of unique chemical interactions between the hydrophobic ions and the transport barriers of the NPC.[52,53] The fouling of a nano-ITIES tip by nuclear proteins will be avoidable using the nucleoplasm-free NE[61] in the future SECM study of single NPCs.

Discovery of the NPC-permeabilizing ions provided unprecedented insights into the gating mechanism of molecular transport through the NPCs. Our finding further supports the hypothesis that the interior of the NPC is nanostructured into central and peripheral routes.[11−14] Moreover, we proposed a new model to explain pathway- and mode-dependent permeabilization of the NPC by the hydrophobic ions. In our model, the NPC possesses tighter mesh barriers in the crowding central route and more flexible polymer-brush barriers in the aqueous peripheral route. Importantly, our synergetic model is consistent with many structural and functional ingredients of the NPC as known experimentally and theoretically. Moreover, our model implies that the peripheral route should be targeted for the efficient nuclear import of macromolecular and nanomaterial therapeutics. The efficient nuclear import of glycosylated plasmids[58,59] and nanoparticles[60] has been demonstrated for gene therapy and nanomedicine, whereas the use of the peripheral route has been unnoticed.

■ AUTHOR INFORMATION

Corresponding Author

*E-mail: amemiya@pitt.edu.

Present Addresses

[†]J.K.: Department of Chemistry and Biochemistry, University of Texas at Austin, Austin, TX 78712.

[§]A.I.: Department of Chemistry and Physics, Arkansas State University, State University, Arkansas 72467.
[¶]M.S.: Department of Chemistry, University of Illinois at Urbana−Champaign, Urbana, Illinois 61801.
[‡]R.I.: Department of Applied Chemistry, Graduate School of Engineering, Kyushu University, Nishi-Ku, Fukuoka 819-0395, Japan.

Author Contributions

[#]J.K. and A.I. equally contributed to this research.

Notes

The authors declare no competing financial interest.

■ ACKNOWLEDGMENTS

This work was supported by the National Institutes of Health (GM073439). We thank Dr. Michael G. Opferman and Prof. Rob D. Coalson, University of Pittsburgh, for their helpful discussions. We also acknowledge the Petersen Institute of NanoScience and Engineering at the University of Pittsburgh for its technical support with FIB milling.

■ REFERENCES

(1) Terry, L. J.; Shows, E. B.; Wente, S. R. *Science* **2007**, *318*, 1412.
(2) Strambio-De-Castillia, C.; Niepel, M.; Rout, M. P. *Nat. Rev. Mol. Cell Biol.* **2010**, *11*, 490.
(3) Pack, D. W.; Hoffman, A. S.; Pun, S.; Stayton, P. S. *Nat. Rev. Drug Discovery* **2005**, *4*, 581.
(4) Raices, M.; D'Angelo, M. A. *Nat. Rev. Mol. Cell Biol.* **2012**, *13*, 687.
(5) Frenkiel-Krispin, D.; Maco, B.; Aebi, U.; Medalia, O. *J. Mol. Biol.* **2010**, *395*, 578.
(6) Zheng, D.; Giljohann, D. A.; Chen, D. L.; Massich, M. D.; Wang, X. Q.; Iordanov, H.; Mirkin, C. A.; Paller, A. S. *Proc. Natl. Acad. Sci. U.S.A.* **2012**, *109*, 11975.
(7) Hoelz, A.; Debler, E. W.; Blobel, G. *Annu. Rev. Biochem.* **2011**, *80*, 613.
(8) Falces, J.; Arregi, I.; Konarev, P. V.; Urbaneja, M. a. A.; Svergun, D. I.; Taneva, S. G.; Bañuelos, S. *Biochemistry* **2010**, *49*, 9756.
(9) Lim, R. Y. H.; Huang, N. P.; Koser, J.; Deng, J.; Lau, K. H. A.; Schwarz-Herion, K.; Fahrenkrog, B.; Aebi, U. *Proc. Natl. Acad. Sci. U.S.A.* **2006**, *103*, 9512.
(10) Frey, S.; Richter, R. P.; Görlich, D. *Science* **2006**, *314*, 815.
(11) Yamada, J.; Phillips, J. L.; Patel, S.; Goldfien, G.; Calestagne-Morelli, A.; Huang, H.; Reza, R.; Acheson, J.; Krishnan, V. V.; Newsam, S.; Gopinathan, A.; Lau, E. Y.; Colvin, M. E.; Uversky, V. N.; Rexach, M. F. *Mol. Cell. Proteomics* **2010**, *9*, 2205.
(12) Liashkovich, I.; Meyring, A.; Oberleithner, H.; Shahin, V. *J. Controlled Release* **2012**, *160*, 601.
(13) Ma, J.; Goryaynov, A.; Sarma, A.; Yang, W. *Proc. Natl. Acad. Sci. U.S.A.* **2012**, *109*, 7326.
(14) Kim, J.; Izadyar, A.; Nioradze, N.; Amemiya, S. *J. Am. Chem. Soc.* **2013**, *135*, 2321.
(15) Chatel, G.; Desai, S. H.; Mattheyses, A. L.; Powers, M. A.; Fahrenkrog, B. *J. Struct. Biol.* **2012**, *177*, 81.
(16) Solmaz, S. R.; Blobel, G.; Melčák, I. *Proc. Natl. Acad. Sci. U.S.A.* **2013**, *110*, 5858.
(17) Hulsmann, B. B.; Labokha, A. A.; Görlich, D. *Cell* **2012**, *150*, 738.
(18) Labokha, A. A.; Gradmann, S.; Frey, S.; Hulsmann, B. B.; Urlaub, H.; Baldus, M.; Görlich, D. *EMBO J.* **2013**, *32*, 204.
(19) Finlay, D. R.; Newmeyer, D. D.; Price, T. M.; Forbes, D. J. *J. Cell Biol.* **1987**, *104*, 189.
(20) Schwefel, D.; Maierhofer, C.; Beck, J. G.; Seeberger, S.; Diederichs, K.; Moller, H. M.; Welte, W.; Wittmann, V. *J. Am. Chem. Soc.* **2010**, *132*, 8704.
(21) Loschberger, A.; van de Linde, S.; Dabauvalle, M. C.; Rieger, B.; Heilemann, M.; Krohne, G.; Sauer, M. *J. Cell Sci.* **2012**, *125*, 570.
(22) Amemiya, S.; Bard, A. J.; Fan, F.-R. F.; Mirkin, M. V.; Unwin, P. R. *Annu. Rev. Anal. Chem.* **2008**, *1*, 95.
(23) Bard, A. J., Mirkin, M. V., Eds. *Scanning Electrochemical Microscopy*, 2nd ed.; CRC Press: Boca Raton, FL, 2012.
(24) Guo, J.; Amemiya, S. *Anal. Chem.* **2005**, *77*, 2147.
(25) Girault, H. H. Electrochemistry at Liquid/Liquid Interfaces. In *Electroanalytical Chemistry*; Bard, A. J., Zoski, C. G., Eds.; Taylor & Francis: Boca Raton, FL, 2010; Vol. *23*, p 1.
(26) Amemiya, S.; Bard, A. J. *Anal. Chem.* **2000**, *72*, 4940.
(27) Ishimatsu, R.; Kim, J.; Jing, P.; Striemer, C. C.; Fang, D. Z.; Fauchet, P. M.; McGrath, J. L.; Amemiya, S. *Anal. Chem.* **2010**, *82*, 7127.
(28) Nioradze, N.; Chen, R.; Kim, J.; Shen, M.; Santhosh, P.; Amemiya, S. *Anal. Chem.* **2013**, 6198.
(29) Elsamadisi, P.; Wang, Y.; Velmurugan, J.; Mirkin, M. V. *Anal. Chem.* **2011**, *83*, 671.
(30) Zhan, D. P.; Fan, F. R. F.; Bard, A. J. *Proc. Natl. Acad. Sci. U.S.A.* **2008**, *105*, 12118.
(31) Ishimatsu, R.; Izadyar, A.; Kabagambe, B.; Kim, Y.; Kim, J.; Amemiya, S. *J. Am. Chem. Soc.* **2011**, *133*, 16300.
(32) Kim, J.; Shen, M.; Nioradze, N.; Amemiya, S. *Anal. Chem.* **2012**, *84*, 3489.
(33) Shen, M.; Ishimatsu, R.; Kim, J.; Amemiya, S. *J. Am. Chem. Soc.* **2012**, *134*, 9856.
(34) Shahin, V.; Ludwig, Y.; Oberleithner, H. Investigation of Nuclear Envelope Structure and Passive Permeability. In *The Nucleus: Chromatin, Transcription, Envelope, Proteins, Dynamics, and Imaging*; Hancock, R., Ed.; Humana Press: New York, 2008; Vol. *2*, p 161.
(35) Wang, Y.; Kececi, K.; Velmurugan, J.; Mirkin, M. V. *Chem. Sci.* **2013**, *4*, 3606.
(36) Jing, P.; Rodgers, P. J.; Amemiya, S. *J. Am. Chem. Soc.* **2009**, *131*, 2290.
(37) Barker, A. L.; Macpherson, J. V.; Slevin, C. J.; Unwin, P. R. *J. Phys. Chem. B* **1998**, *102*, 1586.
(38) Wang, H.; Clapham, D. E. *Biophys. J.* **1999**, *77*, 241.
(39) Kim, E.; Xiong, H.; Striemer, C. C.; Fang, D. Z.; Fauchet, P. M.; McGrath, J. L.; Amemiya, S. *J. Am. Chem. Soc.* **2008**, *130*, 4230.
(40) Amemiya, S.; Wang, Y.; Mirkin, M. V. Nanoelectrochemistry at the Liquid/Liquid Interfaces. In *Specialist Periodical Reports in Electrochemistry*; Compton, R. G., Wadhawan, J. D., Eds.; RSC: Cambridge, UK, 2013; Vol. *12*, p 1.
(41) Quinn, B. M.; van't Hof, P.; Lemay, S. G. *J. Am. Chem. Soc.* **2004**, *126*, 8360.
(42) Boika, A.; Thorgaard, S. N.; Bard, A. J. *J. Phys. Chem. B* **2013**, *117*, 4371.
(43) Görlich, D.; Kutay, U. *Annu. Rev. Cell Dev. Biol.* **1999**, *15*, 607.
(44) Ribbeck, K.; Görlich, D. *EMBO J.* **2002**, *21*, 2664.
(45) Bird, C. H.; Blink, E. J.; Hirst, C. E.; Buzza, M. S.; Steele, P. M.; Sun, J. R.; Jans, S. A.; Bird, P. I. *Mol. Cell. Biol.* **2001**, *21*, 5396.
(46) Kirschner, R. H.; Rusli, M.; Martin, T. E. *J. Cell Biol.* **1977**, *72*, 118.
(47) Meyerhoff, M. E.; Fu, B.; Bakker, E.; Yun, J.-H.; Yang, V. C. *Anal. Chem.* **1996**, *68*, 168A.
(48) Eisele, N. B.; Labokha, A. A.; Frey, S.; Görlich, D.; Richter, R. P. *Biophys. J.* **2013**, *105*, 1860.
(49) Schoch, R. L.; Kapinos, L. E.; Lim, R. Y. H. *Proc. Natl. Acad. Sci. U.S.A.* **2012**, *109*, 16911.
(50) Milles, S.; Bui, K. H.; Koehler, C.; Eltsov, M.; Beck, M.; Lemke, E. A. *EMBO Rep.* **2013**, *14*, 178.
(51) Frey, S.; Görlich, D. *Cell* **2007**, *130*, 512.
(52) Opferman, M. G.; Coalson, R. D.; Jasnow, D.; Zilman, A. *Phys. Rev. E* **2012**, *86*, 031806.
(53) Opferman, M. G.; Coalson, R. D.; Jasnow, D.; Zilman, A. *Langmuir* **2013**, *29*, 8584.
(54) Powers, M. A.; Forbes, D. J.; Dahlberg, J. E.; Lund, E. *J. Cell Biol.* **1997**, *136*, 241.
(55) Ren, Y.; Seo, H.-S.; Blobel, G.; Hoelz, A. *Proc. Natl. Acad. Sci. U.S.A.* **2010**, *107*, 10406.

(56) Naim, B.; Zbaida, D.; Dagan, S.; Kapon, R.; Reich, Z. *EMBO J.* **2009**, *28*, 2697.
(57) Duverger, E.; Pellerinmendes, C.; Mayer, R.; Roche, A. C.; Monsigny, M. *J. Cell Sci.* **1995**, *108*, 1325.
(58) Fajac, I.; Grosse, S.; Briand, P.; Monsigny, M. *Gene Ther.* **2002**, *9*, 740.
(59) Akita, H.; Masuda, T.; Nishio, T.; Niikura, K.; Ijiro, K.; Harashima, H. *Mol. Pharmaceutics* **2011**, *8*, 1436.
(60) Sekiguchi, S.; Niikura, K.; Matsuo, Y.; Yoshimura, S. H.; Ijiro, K. *RSC Adv.* **2012**, *2*, 1656.
(61) Herrmann, M.; Neuberth, N.; Wissler, J.; Perez, J.; Gradl, D.; Naber, A. *Nano Lett.* **2009**, *9*, 3330.